

7.4. CORRECTION OF SYSTEMATIC ERRORS

wavevectors on one sheet correspond to scattering with phonon emission and on the other sheet to phonon absorption. For $\beta > 1$, the conic section is an ellipsoid with P at one focus. Scattering now occurs either by emission or by absorption, but not by both together (Fig. 7.4.2.3).

To evaluate the TDS correction, with \mathbf{q} restricted to lie along the scattering surfaces, separate treatments are required for faster-than-sound ($\beta < 1$) and for slower-than-sound ($\beta > 1$) neutrons. The final results can be summarized as follows (Willis, 1970; Cooper, 1971):

- (a) For faster-than-sound neutrons, the TDS rises to a maximum, just as for X-rays, and the correction factor is given by (7.4.2.13), which applies to the X-ray case. (This is a remarkable result in view of the marked difference in the one-phonon scattering surfaces for X-rays and neutrons.)
- (b) For slower-than-sound neutrons, the correction factor depends on the velocity (wavelength) of the neutrons and is more difficult to evaluate than in (a). However, α will always be less than that calculated for X-rays of the same wavelength, and under certain conditions the TDS does not rise to a maximum at all so that α is then zero.

The sharp distinction between cases (a) and (b) has been confirmed experimentally using the neutron Laue technique on single-crystal silicon (Willis, Carlile & Ward, 1986).

7.4.2.4. Correction factor for powders

Thermal diffuse scattering in X-ray powder-diffraction patterns produces a non-uniform background that peaks sharply at the positions of the Bragg reflections, as in the single-crystal case (see Fig. 7.4.2.4). For a given value of the scattering vector, the one-phonon TDS is contributed by all those wavevectors \mathbf{q} joining the reciprocal-lattice point and any point on the surface of a sphere of radius $2 \sin \theta / \lambda$ with its centre at the origin of reciprocal space. These \mathbf{q} vectors reach the boundary of the Brillouin zone and are not restricted to those in the neighbourhood of the reciprocal-lattice point. To calculate α properly, we require a knowledge, therefore, of the lattice dynamics of the crystal and not just its elastic properties. This is one reason why relatively little progress has been made in calculating the X-ray correction factor for powders.

7.4.3. Compton scattering

(By N. G. Alexandropoulos and M. J. Cooper)

7.4.3.1. Introduction

In many diffraction studies, it is necessary to correct the intensities of the Bragg peaks for a variety of inelastic scattering processes. Compton scattering is only one of the incoherent processes although the term is often used loosely to include plasmon, Raman, and resonant Raman scattering, all of which may occur in addition to the more familiar fluorescence radiation and thermal diffuse scattering. The various interactions are summarized schematically in Fig. 7.4.3.1, where the dominance of each interaction is characterized by the energy and momentum transfer and the relevant binding energy.

With the exception of thermal diffuse scattering, which is known to peak at the reciprocal-lattice points, the incoherent background varies smoothly through reciprocal space. It can be removed with a linear interpolation under the sharp Bragg peaks and without any energy analysis. On the other hand, in non-crystalline material, the elastic scattering is also diffused throughout reciprocal space; the point-by-point correction is consequently larger and without energy analysis it cannot be made empirically; it must be calculated. These calculations are

Table 7.4.3.1. The energy transfer, in eV, in the Compton scattering process for selected X-ray energies

Scattering angle φ (°)	Cr $K\alpha$ 5411 eV	Cu $K\alpha$ 8040 eV	Mo $K\alpha$ 17 443 eV	Ag $K\alpha$ 22 104 eV
0	0	0	0	0
30	8	17	79	127
60	29	63	292	467
90	57	124	575	915
120	85	185	849	1344
150	105	229	1043	1648
180	112	245	1113	1757

Data calculated from equation (7.4.3.1).

imprecise except in the situations where Compton scattering is the dominant process. For this to be the case, there must be an encounter, conserving energy and momentum, between the incoming photon and an individual target electron. This in turn will occur if the energy lost by the photon, $\Delta E = E_1 - E_2$, clearly exceeds the one-electron binding energy, E_B , of the target electron. Eisenberger & Platzman (1970) have shown that this binary encounter model – alternatively known as the impulse approximation – fails as $(E_B/\Delta E)^2$.

The likelihood of this failure can be predicted from the Compton shift formula, which for scattering through an angle φ can be written.

$$\Delta E = E_1 - E_2 = \frac{E_1^2(1 - \cos \varphi)}{mc^2[1 + (E_1/mc^2)(1 - \cos \varphi)]}. \quad (7.4.3.1)$$

This energy transfer is given as a function of the scattering angle in Table 7.4.3.1 for a set of characteristic X-ray energies; it ranges from a few eV for Cr $K\alpha$ X-radiation at small angles, up to ~ 2 keV for backscattered Ag $K\alpha$ X-radiation. Clearly, in the majority of typical experiments Compton scattering will be inhibited from all but the valence electrons.

7.4.3.2. Non-relativistic calculations of the incoherent scattering cross section

7.4.3.2.1. Semi-classical radiation theory

For weak scattering, treated within the Born approximation, the incoherent scattering cross section, $(d\sigma/d\Omega)_{\text{inc}}$, can be factorized as follows:

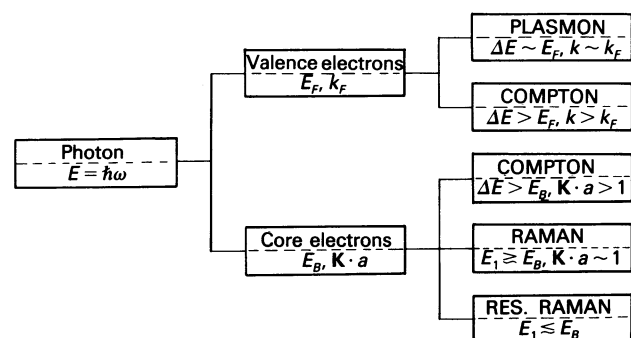


Fig. 7.4.3.1. Schematic diagram of the inelastic scattering interactions, $\Delta E = E_1 - E_2$ is the energy transferred from the photon and \mathbf{K} the momentum transfer. The valence electrons are characterized by the Fermi energy, E_F , and momentum, k_F (\hbar being taken as unity). The core electrons are characterized by their binding energy E_B . The dipole approximation is valid when $|\mathbf{K}|a < 1$, where a is the orbital radius of the scattering electron.

7. MEASUREMENT OF INTENSITIES

Table 7.4.3.2. *The incoherent scattering function for elements up to Z = 55*

Element	$(\sin \theta)/\lambda$ (\AA^{-1})											
	0.10	0.20	0.30	0.40	0.50	0.60	0.70	0.80	0.90	1.00	1.50	2.00
1 H	0.343	0.769	0.937	0.983	0.995	0.998	0.994	0.999	1.000	1.000	1.000	1.000
2 He	0.296	0.881	1.362	1.657	1.817	1.902	1.947	1.970	1.983	1.990	1.999	2.000
3 Li	1.033	1.418	1.795	2.143	2.417	2.613	2.746	2.834	2.891	2.928	2.989	2.998
4 Be	1.170	2.121	2.471	2.744	3.005	3.237	3.429	3.579	3.693	3.777	3.954	3.989
5 B	1.147	2.531	3.190	3.499	3.732	3.948	4.146	4.320	4.469	4.590	4.895	4.973
6 C	1.039	2.604	3.643	4.184	4.478	4.690	4.878	5.051	5.208	5.348	5.781	5.930
7 N	1.08	2.858	4.097	4.792	5.182	5.437	5.635	5.809	5.968	6.113	6.630	6.860
8 O	0.977	2.799	4.293	5.257	5.828	6.175	6.411	6.596	6.755	6.901	7.462	7.764
9 F	0.880	2.691	4.347	5.552	6.339	6.832	7.151	7.376	7.552	7.703	8.288	8.648
10 Ne	0.812	2.547	4.269	5.644	6.640	7.320	7.774	8.085	8.312	8.490	9.113	9.517
11 Na	1.503	2.891	4.431	5.804	6.903	7.724	8.313	8.729	9.028	9.252	9.939	10.376
12 Mg	2.066	3.444	4.771	6.064	7.181	8.086	8.784	9.304	9.689	9.975	10.766	11.229
13 Al	2.264	4.047	5.250	6.435	7.523	8.459	9.225	9.830	10.296	10.652	11.592	12.083
14 Si	2.293	4.520	5.808	6.903	7.937	8.867	9.667	10.330	10.864	11.286	12.408	12.937
15 P	2.206	4.732	6.312	7.435	8.419	9.323	10.131	10.827	11.411	11.888	13.209	13.790
16 S	2.151	4.960	6.795	8.002	8.960	9.829	10.626	11.336	11.952	12.472	13.990	14.641
17 Cl	2.065	5.074	7.182	8.553	9.539	10.382	11.158	11.867	12.499	13.050	14.750	15.487
18 Ar	1.956	5.033	7.377	8.998	10.106	10.967	11.726	12.424	13.061	13.629	15.489	16.324
19 K	2.500	5.301	7.652	9.405	10.650	11.568	12.329	13.014	13.645	14.220	16.212	17.152
20 Ca	3.105	5.690	7.981	9.790	11.157	12.163	12.953	13.635	14.256	14.830	16.921	17.970
21 Sc	3.136	5.801	8.169	10.071	11.561	12.648	13.545	14.256	14.885	15.460	17.630	18.782
22 Ti	3.114	5.860	8.312	10.304	11.901	13.140	14.093	14.856	15.509	16.095	18.334	19.585
23 V	3.067	5.858	8.375	10.454	12.156	13.514	14.574	15.413	16.111	16.721	19.032	20.379
24 Cr	2.609	5.577	8.206	10.415	12.264	13.770	14.960	15.902	16.670	17.323	19.730	21.168
25 Mn	2.949	5.791	8.380	10.604	12.486	14.062	15.346	16.376	17.211	17.910	20.411	21.938
26 Fe	2.891	5.781	8.432	10.733	12.687	14.343	15.716	16.831	17.737	18.488	21.097	22.704
27 Co	2.832	5.764	8.469	10.844	12.867	14.596	16.050	17.249	18.229	19.039	21.777	23.462
28 Ni	2.772	5.726	8.461	10.894	12.980	14.780	16.317	17.602	18.664	19.543	22.445	24.211
29 Cu	2.348	5.455	8.310	10.778	12.942	14.847	16.494	17.885	19.043	20.002	23.107	24.957
30 Zn	2.654	5.631	8.388	10.901	13.094	15.020	16.709	18.163	19.395	20.427	23.745	25.683
31 Ga	2.791	5.939	8.599	11.082	13.290	15.233	16.947	18.445	19.734	20.831	24.370	26.400
32 Ge	2.839	6.229	8.912	11.338	13.536	15.486	17.215	18.741	20.074	21.224	24.983	27.109
33 As	2.793	6.365	9.236	11.658	13.828	15.775	17.511	19.056	20.420	21.612	25.583	27.810
34 Se	2.799	6.589	9.601	12.033	14.168	16.098	17.835	19.391	20.778	22.003	26.171	28.504
35 Br	2.771	6.748	9.940	12.440	14.552	16.456	18.185	19.747	21.149	22.399	26.747	29.190
36 Kr	2.703	6.760	10.157	12.828	14.969	16.849	18.562	20.123	21.535	22.804	27.313	29.870
37 Rb	3.225	7.062	10.431	13.206	15.410	17.282	18.974	20.526	21.940	23.221	27.871	30.543
38 Sr	3.831	7.464	10.746	13.576	15.860	17.745	19.420	20.956	22.367	23.654	28.423	31.210
39 Y	3.999	7.700	11.010	13.899	16.279	18.215	19.891	21.416	22.820	24.110	28.970	31.870
40 Zr	4.064	7.879	11.236	14.176	16.658	18.672	20.373	21.895	23.294	24.583	29.517	32.522
41 Nb	3.672	7.684	11.213	14.317	16.949	19.081	20.844	22.386	23.787	25.077	30.067	33.167
42 Mo	3.625	7.690	11.260	14.444	17.196	19.455	21.300	22.877	24.288	25.581	30.620	33.808
43 Tc	3.987	7.984	11.512	14.653	17.456	19.816	21.748	23.370	24.797	26.093	31.173	34.447
44 Ru	3.559	7.857	11.531	14.782	17.685	20.150	22.172	23.855	25.312	26.621	31.740	35.081
45 Rh	3.499	7.863	11.591	14.883	17.858	20.428	22.557	24.318	25.819	27.148	32.309	35.715
46 Pd	3.103	7.725	11.441	14.824	17.943	20.653	22.904	24.756	26.316	27.677	32.888	36.349
47 Ag	3.362	7.785	11.598	14.969	18.082	20.858	23.212	25.162	26.792	28.195	33.465	36.983
48 Cd	3.700	7.980	11.812	15.185	18.263	21.064	23.501	25.546	27.252	28.705	34.046	37.618
49 In	3.852	8.297	12.083	15.444	18.489	21.288	23.779	25.906	27.691	29.203	34.634	38.255
50 Sn	3.917	8.615	12.415	15.746	18.760	21.541	24.059	26.252	28.113	29.687	35.226	38.894
51 Sb	3.871	8.811	12.777	16.088	19.067	21.823	24.349	26.590	28.518	30.157	35.822	39.536
52 Te	3.097	9.076	13.171	16.466	19.407	22.134	25.655	26.927	28.912	30.613	36.422	40.181
53 I	3.903	9.287	13.564	16.876	19.227	22.471	24.980	27.269	29.298	31.056	37.024	40.827
54 Xe	3.841	9.340	13.892	17.307	20.175	22.833	25.324	27.619	29.680	31.488	37.628	41.477
55 Cs	4.320	9.615	14.217	17.753	20.612	23.228	25.691	27.981	30.064	31.914	38.232	42.129

$$\left(\frac{d\sigma}{d\Omega}\right)_{\text{inc}} = \left(\frac{d\sigma}{d\Omega}\right)_0 S(E_1, E_2, \mathbf{K}, Z), \quad (7.4.3.2)$$

where $(d\sigma/d\Omega)_0$ is the cross section characterizing the interaction, in this case it is the Thomson cross section, $(e^2/mc^2)^2 \boldsymbol{\varepsilon}_1 \cdot \boldsymbol{\varepsilon}_2$; $\boldsymbol{\varepsilon}_1$ and $\boldsymbol{\varepsilon}_2$ being the initial and final state photon

polarization vectors. The dynamics of the target are contained in the incoherent scattering factor $S(E_1, E_2, \mathbf{K}, Z)$, which is usually a function of the energy transfer $\Delta E = E_1 - E_2$, the momentum transfer \mathbf{K} , and the atomic number Z .

The electromagnetic wave perturbs the electronic system through the vector potential \mathbf{A} in the Hamiltonian

7.4. CORRECTION OF SYSTEMATIC ERRORS

$$H = \frac{e}{me} \mathbf{p} \cdot \mathbf{A} + \frac{e^2}{2me^2} \mathbf{A} \cdot \mathbf{A}. \quad (7.4.3.3)$$

It produces photoelectric absorption through the $\mathbf{p} \cdot \mathbf{A}$ term taken in first order, Compton and Raman scattering through the $\mathbf{A} \cdot \mathbf{A}$ term and resonant Raman scattering through the $\mathbf{p} \cdot \mathbf{A}$ terms in second order.

If resonant scattering is neglected for the moment, the expression for the incoherent scattering cross section becomes

$$S = \sum_f (E_2/E_1)^2 \left| \langle \psi_f | \sum_j \exp(i\mathbf{K} \cdot \mathbf{r}_j) | \psi_i \rangle \right|^2 \delta(E_f - E_i - \Delta E), \quad (7.4.3.4)$$

where the Born operator is summed over the j target electrons and the matrix element is summed over all final states accessible through energy conservation. In the high-energy limit of $\Delta E \gg E_B$, $S(E_1, E_2, \mathbf{K}, Z) \rightarrow Z$ but as Table 7.4.3.1 shows this condition does not hold in the X-ray regime.

The evaluation of the matrix elements in equation (7.4.3.4) was simplified by Waller & Hartree (1929) who (i) set $E_2 = E_1$ and (ii) summed over all final states irrespective of energy conservation. Closure relationships were then invoked to reduce the incoherent scattering factor to an expression in terms of form factors f_{jk} :

$$S = \sum_j [1 - |f_j(\mathbf{K})|^2] - \sum_j \sum_{k \neq j} |f_{jk}(\mathbf{K})|^2, \quad (7.4.3.5)$$

where

$$f_j(\mathbf{K}) = \langle \psi_j | \exp(i\mathbf{K} \cdot \mathbf{r}_j) | \psi_j \rangle$$

and

$$f_{jk} = \langle \psi_k | \exp[i\mathbf{K} \cdot (\mathbf{r}_k - \mathbf{r}_j)] | \psi_j \rangle,$$

the latter term arising from exchange in the many-electron atom.

According to Currat, DeCicco & Weiss (1971), equation (7.4.3.5) can be improved by inserting the prefactor $(E_2/E_1)^2$, where E_2 is calculated from equation (7.4.3.1); the factor is an average for the factors inside the summation sign of equation (7.4.3.4) that were neglected by Waller & Hartree. This term has been included in a few calculations of incoherent intensities [see, for example, Bloch & Mendelsohn (1979)]. The Waller-Hartree method remains the chosen basis for the most extensive compilations of incoherent scattering factors, including those tabulated here, which were calculated by Cromer & Mann (1967) and Cromer (1969) from non-relativistic Hartree-Fock self-consistent-field wavefunctions. Table 7.4.3.2 is taken from the compilation by Hubbell, Veigele, Briggs, Brown, Cromer & Howerton (1975).

7.4.3.2.2. Thomas-Fermi model

This statistical model of the atomic charge density (Thomas, 1927; Fermi, 1928) considerably simplifies the calculation of coherent and incoherent scattering factors since both can be written as universal functions of \mathbf{K} and Z . Numerical values were first calculated by Bewilogua (1931); more recent calculations have been made by Brown (1966) and Veigele (1967). The method is less accurate than Waller-Hartree theory, but it is a much simpler computation.

7.4.3.2.3. Exact calculations

The matrix elements of (7.4.3.4) can be evaluated exactly for the hydrogen atom. If one-electron wavefunctions in many-electron atoms are modelled by hydrogenic orbitals [with a

Table 7.4.3.3. Compton scattering of Mo $K\alpha$ X-radiation through 170° from $2s$ electrons

Element	S_{exact}	S_{imp}	$S_{\text{W-H}}$
Li	0.879	0.878	0.877
B	0.879	0.878	0.877
O	0.878	0.877	0.876
Ne	0.875	0.875	0.875
Mg	0.863	0.863	0.872
Si	0.851	0.850	0.868
Ar	0.843	0.826	0.877
V	0.663	0.716	0.875
Cr	0.568	0.636	0.875

S_{exact} is the incoherent scattering factor calculated analytically from a hydrogenic atomic model. S_{imp} is the incoherent scattering factor calculated by taking the Compton profile derived in the impulse approximation and truncating it for $\Delta E < E_B$. $S_{\text{W-H}}$ is the Waller-Hartree incoherent scattering factor. Data taken from Bloch & Mendelsohn (1974).

suitable choice of the orbital exponent; see, for example, Slater (1937)], an analytical approach can be used, as was originally proposed by Bloch (1934).

Hydrogenic calculations have been shown to predict accurate K - and L -shell photoelectric cross sections (Pratt & Tseng, 1972). The method has been applied in a limited number of cases to K -shell (Eisenberger & Platzman, 1970) and L -shell (Bloch & Mendelsohn, 1974) incoherent scattering factors, where it has served to highlight the deficiencies of the Waller-Hartree approach. In chromium, for example, at an incident energy of ~ 17 keV and a Bragg angle of 85° , the L -shell Waller-Hartree cross section is higher than the 'exact' calculation by $\sim 50\%$. A comparison of Waller-Hartree and exact results for $2s$ electrons, taken from Bloch & Mendelsohn (1974), is given in Table 7.4.3.3 for illustration. The discrepancy is much reduced when all electrons are considered.

In those instances where the exact method has been used as a yardstick, the comparison favours the 'relativistic integrated impulse approximation' outlined below, rather than the Waller-Hartree method.

7.4.3.3. Relativistic treatment of incoherent scattering

The Compton effect is a relativistic phenomenon and it is accordingly more satisfactory to start from this basis, *i.e.* the Klein & Nishina (1929) theory and the Dirac equation (see Jauch & Rohrlich, 1976). In second-order relativistic perturbation theory, there is no overt separation of $\mathbf{p} \cdot \mathbf{A}$ and $\mathbf{A} \cdot \mathbf{A}$ terms. The inclusion of electron spin produces additional terms in the Compton cross section that depend upon the polarization (Lipps & Tolhoek, 1954); they are generally small at X-ray energies. They are of increasing interest in synchrotron-based experiments where the brightness of the source and its polarization characteristics compensate for the small cross section (Blume & Gibbs, 1988).

Somewhat surprisingly, it is the spectral distribution, $d^2\sigma/d\Omega dE_2$, rather than the total intensity, $d\sigma/d\Omega$, which is the better understood. This is a consequence of the exploitation of the Compton scattering technique to determine electron momentum density distributions through the Doppler broadening of the scattered radiation [see Cooper (1985) and Williams (1977) for reviews of the technique]. Manninen, Paakkari & Kajantie (1976) and Ribberfors (1975) have shown that the